CHARACTERIZING LUNAR REGOLITH, EMPLACEMENT AND DEGRADATION PROCESSES ASSOCIATED WITH IMPACT FEATURES. M. Alexandra Matiella Novak[1], G. Wesley Patterson[1], Benjamin T. Greenhagen[1], Joshua T. S. Cahill [1]Johns Hopkins University Applied Physics Laboratory, 11100 Johns Hopkins Rd. Laurel, MD 20723.

Introduction: There is a discrepancy that exists among some features that have been determined to be of Imbrian, or older, age, but display regolith properties, such as the presence of surface boulders, that are more consistent with features that are much younger. For example, while Copernican aged craters have rocky ejecta that degrades at a predictable rate [1], Tsiolkovskiy crater (>3.2 Ga), has a unique surface rock population higher than expected for a crater of its size and age [2]. Furthermore studies have show variation in the correlation of Diviner Lunar Radiometer (Diviner) thermal infrared rock abundance data to Miniature Radio Frequencey (Mini-RF) radar surface roughness data and demonstrated the differing rates of regolith degradation at the surface and sub-surface [1]These initial studies suggest that the physical properties of features of different ages manifest differently depending on the wavelength region used in analysis. Integrating an analysis of radar, thermal and image data to physically characterize these features will help us to better constrain processes that control regolith formation and evolution, both at the surface and in the sub-surface. Our main objective is to develop a methodology that integrates Mini-RF roughness, Diviner rock abundance, and LROC imagery boulder counting to provide more robust constraints on the relative ages and degradation rates of regolith through the physical characterization of lunar features of different ages, such as crater ejecta, crater impact melts, mare, and large ray systems. Here we focus on preliminary analysis looking at impact features (ejecta and melt).

Background: When studying regolith associated with cratering processes, we can focus our studies on impact crater features such as melt-free ejecta, melt ponds, ejecta with melt flows, and floor of the crater away from the walls. All of these features give us access to regolith at centimeter to meter scales, and an opportunity to understand how regolith for each feature type degrades. Using LRO data, [2] investigated the age-dependent characteristics of crater ejecta as a measure of rock degradation rates. Based on Diviner rock abundance, the results implied shorter rock survival times than predicted based on downward extrapolation of 100 m crater size frequency. They concluded that all surface rocks disappear over a period of roughly 1 byr and that for older craters the ejecta that remains exists within the subsurface, i.e., not visible to Diviner.

Methods: The suite of instruments onboard the NASA Lunar Reconnaissance Orbiter (LRO) are providing much needed global observations capable of better informing us on lunar surface physical properties such as surface roughness and rock abundance at both the surface and at modest depths into the regolith [3].

Lunar Data Products. Mini-RF is a hybrid polarized, side-looking, synthetic aperture radar (SAR) that primarily transmitted and collected S-band (12.6 cm) observations in a "zoom" mode (15 x 30 m resolution) [3]. Mini-RF provides a unique means to analyze the surface and subsurface physical properties of geologic deposits, including their wavelength-scale roughness, the relative depth of the deposits, and some limited compositional information. The most common product derived and used from radar for analysis is the circular polarization ratio (CPR). This product serves as a measure of surface roughness and is defined as the ratio of the backscattered power in the same-sense (SC) polarization that was transmitted relative to the backscattered power in the opposite-sense (OC) polarization returned to the instrument receiver.

Diviner's rock abundance estimates leverage the wavelength dependence of thermal emission for scenes of mixed temperatures. Bandfield and coworkers [4] produced a model for simultaneously solving for the areal fraction of rocks greater than ~0.5 to 1 m in diameter and the temperature of the rock-free regolith using thermal models and nighttime data from three of Diviner's broad thermal channels: Ch. 6 (13–23 μm), Ch. 7 (26–41 μm), and Ch. 8 (50–100 μm). We will be using global 128 pixels per degree maps of Diviner rock abundance for our analysis.

Thermal and radar analysis and interpretation will be enhanced with LROC Narrow-Angle Camera (NAC) observations. The NAC consists of two monochrome line scan imagers with resolutions of 0.5 m/pixel. These images will be critical for additional geologic context and high spatial resolution. We will employ these data in combination with Mini-RF and Diviner to assess the physical properties of impact featuers observed more readily at the surface. Additionally, we will use NAC imagery for our size-frequency boulder counting effort. Meter-scale boulders observed in LROC data would be an accurate representation of meter-scale scatterers in CPR data. This helps constrain our observations and may produce a better means of assessing whether CPR can discriminate relative age.

Target Selections. Target selections for this work are based on previous work on impact melts and ejecta degradation rates. Recent research on crater features,

such as impact ejecta, impact melt, and degradation rates [1,5,6] will be consulted for target areas that have rates [1,2,5,6] wiil be consulted for target areas that have been studied using Mini-RF and Diviner data. A new survey of impact melt flows in the Mini-RF data set provides a more complete global picture of these flow features, providing insight on fundamental questions about the emplacement of melt during the impact cratering process [5]. Ghent and coworkers [6] investigated the physical properties, and changes through time, of lunar impact ejecta using radar and thermal infrared data for craters associated with a variety of ages, while Greenhagen and coworders [2] analyzed the origin of anomalously rocky appearance of Tsiolkovskiy crater and compared it to craters of similar size that are older (e.g., Humboldt) and craters of similar age that are smaller (e.g., Theophilus and Langrenus).

Preliminary Results: Here we present preliminary results from integrating analysis of radar, thermal and image data to physically characterize impact features associated with Hesiodus E crater (~3 km diameter). Figure 1 is a Mini-RF CPR image showing the surface roughness of Hesioudus E and surrounding regolith. As expected, the ejecta surrounding this crater is rougher than the surrounding terrain. Additionally, melt flows within the ejecta were documented by Denevi and coworkders [7].

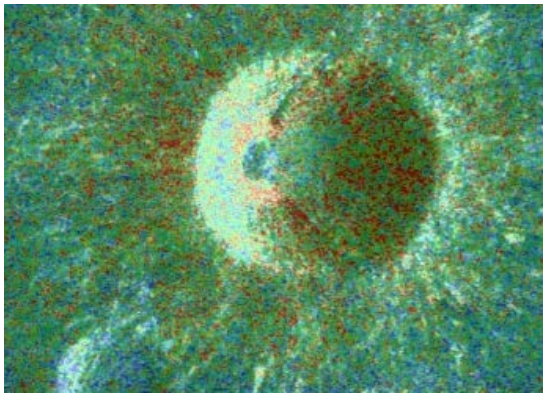

Figure 1. Hesiodus E Crater in Mini-RF CPR data. Bright yellow colors correspond with greater CPR roughness values.

Figure 2 is a global rock abundance map, produced from Diviner data, centered on Hesiodus E. Areas of greater rock abundance are on the floor of the crater and within an area of ejecta to the WSW of the crater. These higher RA values correspond to areas where impact melt exists within the ejecta. Looking at the region more closely in LROC NAC imagery (Figure 3), we can see the area is populated with hundreds of boulders ranging in size from about 1 m to about 25 m across the longest axis. Additionally, bands of boulders seem to be concentrated within higher albedo areas. We will continue integrating these data sets in order to better constrain the physical characteristics of these types of features for both emplacement and degradation processes.

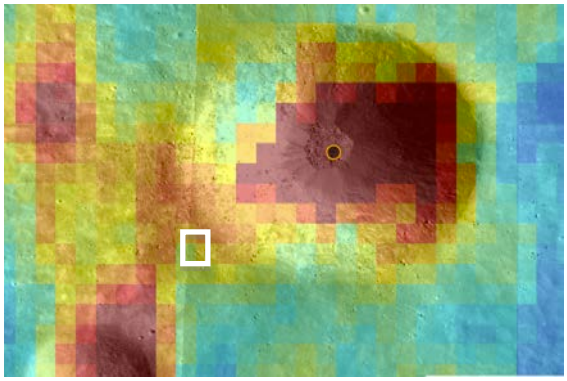

Figure 2. Diviner Rock Abundance map for Hesiodus E. The region within the white box is enlarged as a LROC NAC image in Figure 3.

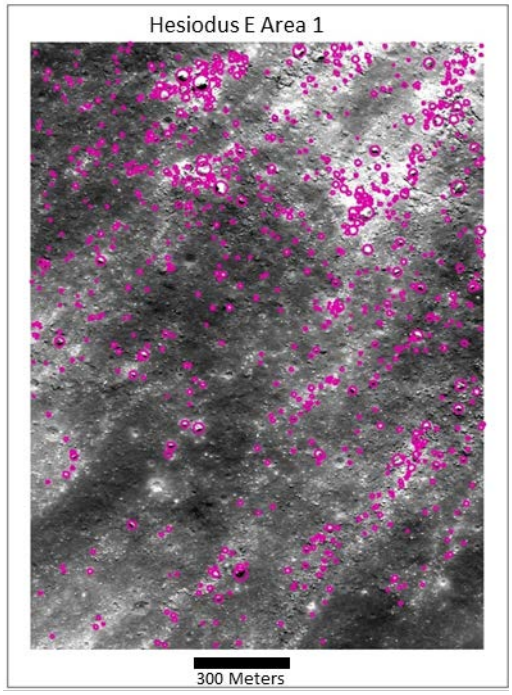

Figure 3. LROC NAC image used for bolder size-frequency counts. Boulders are circled in pink. The black scale bar is 300 m long.

References: [1] Ghent et al. (2014) *Geology, 42 (12),* 1059-1062. [2] Greenhagen et al. (2016) *Icarus, 273,* 237-247.[3] Cahill et al. (2014) *Icarus, 243,* 173-190. [4] Bandfield et al. (2011) *J. Geophys. Res., 116.* [5] Neish et al. (2014) *Icarus, 239,* 105-117. [6] Ghent et al. (2016) *Icarus, 273,* 182-195. [7] Denevi et al. (2012) *Icarus, 219,* 665-675.